Article

Virtual Screening and Hit Selection of Natural Compounds as Acetylcholinesterase Inhibitors

Mariyana Atanasova [1,*] , **Ivan Dimitrov** [1] , **Stefan Ivanov** [1,2] , **Borislav Georgiev** [3] , **Strahil Berkov** [3] , **Dimitrina Zheleva-Dimitrova** [1] and **Irini Doytchinova** [1]

[1] Chemistry Department, Faculty of Pharmacy, Medical University of Sofia, 1000 Sofia, Bulgaria; idimitrov@pharmfac.mu-sofia.bg (I.D.); stefan@redesignscience.com (S.I.); dzheleva@pharmfac.mu-sofia.bg (D.Z.-D.); idoytchinova@pharmfac.mu-sofia.bg (I.D.)

[2] Redesign Science, 180 Varick St, New York, NY 10014, USA

[3] Institute of Biodiversity and Ecosystem Research, Bulgarian Academy of Sciences, 1113 Sofia, Bulgaria; bobogeorgiev5@gmail.com (B.G.); berkov_str@yahoo.com (S.B.)

* Correspondence: matanasova@pharmfac.mu-sofia.bg

Abstract: Acetylcholinesterase (AChE) is one of the classical targets in the treatment of Alzheimer's disease (AD). Inhibition of AChE slows down the hydrolysis of acetycholine and increases choline levels, improving the cognitive function. The achieved success of plant-based natural drugs acting as AChE inhibitors, such as galantamine (GAL) from Galanthus genus and huperzine A from Huperzia serrate (approved drug in China), in the treatment of AD, and the fact that natural compounds (NCs) are considered as safer and less toxic compared to synthetic drugs, led us to screen the available NCs (almost 150,000) in the ZINC12 database for AChE inhibitory activity. The compounds were screened virtually by molecular docking, filtered for suitable ADME properties, and 32 ligands from 23 structural groups were selected. The stability of the complexes was estimated via 1 μs molecular dynamics simulation. Ten compounds formed stable complexes with the enzyme and had a vendor and a reasonable price per mg. They were tested for AChE inhibitory and antioxidant activity. Five compounds showed weak AChE inhibition and three of them exhibited high antioxidant activity.

1. Introduction

Neurodegenerative diseases are characterized by the progressive and irreversible loss of neurons from specific regions in the brain. Alzheimer's disease (AD) is associated with a degeneration of hippocampal and cortical neurons due to the overproduction of cytotoxic β-amyloid (Aβ) peptides followed by an extracellular formation of plaques and intracellular deposition of hyperphosphorylated tau (τ) protein-forming neurofibrillary tangles (NFTs) [1,2]. Neuronal death leads to a reduction in acetylcholine (ACh) levels in synaptic clefts expressed by short-term memory loss and impairment in thinking, speaking, learning, orientation, judgment, and communication [1,3,4]. Cognitive dysfunction is related to two biochemical factors—continuous loss of neurotransmitter ACh due to hyperactivity of the enzyme acetylcholinesterase (AChE) responsible for breaking down ACh into choline, and hyperactive N-methyl-D-aspartate (NMDA) glutamate receptors [5]. One of the therapeutic approaches to AD is the inhibition of AChE, leading to an increase in ACh levels and amelioration of the cognitive function.

The binding site (BS) of AChE is well studied. It is a deep and narrow gorge consisting of several domains: catalytic, anionic, acyl, oxyanion, and peripheral anionic [6–11]. The most important among them are catalytic anionic site (CAS) at the bottom of the BS and the peripheral anionic site (PAS) at the entrance and the gorge. PAS is responsible for the initial recognition of the positively charged substrate by Tyr72, Asp74, Tyr124, Trp286, and Tyr341.

PAS also is capable of allosterically modulating the activity of the catalytic surface [12]. Additionally, PAS is involved in non-cholinergic functions such as amyloidosis [13], neurite outgrowth, and cell adhesion [14,15]. The substrate trapped by PAS is guided by the other domains to reach CAS. The selective binding to ACh is determined by the acyl subsite consisting of the bulky residues Phe295 and Phe297. The quaternary trimethylammonium choline moiety of ACh forms cation–π interactions with the aromatic residues of the anionic domain—Trp86, Tyr133, Tyr337, and Phe338. In the oxyanion part, constructed by Gly121, Gly122, and Ala204, the substrate tetrahedral transition state is stabilized by a hydrogen-bond network formed between the adopted structural water molecule and the enzyme. The catalytic triad—Ser203, Glu334, and His447 of CAS performs the hydrolysis of ACh by the double-displacement mechanism [16,17].

The AChE inhibitors (AChEIs) marketed currently include donepezil (trade name Aricept), rivastigmine (trade name Exelon), galantamine (GAL) (trade name Reminyl and Nivalin), and tacrine [18]. The first approved drugs for AD treatment tacrine and donepezil have synthetic origin. Tacrine is rarely prescribed due to its hepatotoxicity [19–21] and contentious efficacy [22]. Rivastigmine, approved by the FDA in 2000, is designed from physostigmine—a plant alkaloid isolated from *Physostigma venenosum* [23]. In 2001, GAL, an alkaloid from *Galanthus* genus, was approved for AD treatment [24]. Huperzine A, an alkaloid from *Huperzia serrate*, is used as a dietary supplement for memory function improvement in the USA and has been approved for AD treatment in China [25,26].

Natural compounds (NCs) are often assumed to have better tolerance and safety than synthetic molecules, although side effects including allergic reactions, toxicity, and interactions with drugs have been reported for many products [27,28]. Two of the five currently approved drugs for AD treatment have natural origin. Additionally, there are several extensive reviews on natural AChEIs originating from plants, marine organisms, and fungi [29–34]. The major groups of compounds with AChE inhibitory activity are alkaloids, coumarines, flavonoids, stilbenes, and terpenoids [29–36].

Computer-aided drug design is a powerful technique for the design of new drugs. Structure-based design, including molecular docking (MD), virtual screening (VS) and molecular dynamics simulations (MDS), is widely used for deep understanding of the intimate mechanisms of ligand–protein interactions, discovering hits and leads from massive databases and design of new ligands. Docking studies of small group plant-based alkaloids on AChE revealed pleiocarpine as the most promising and potent AChE antagonist [37]. Similarly, 100 terpenoids collected from different sources were analyzed for their inhibitory activity on AChE and amyloid beta peptide via docking and MDS [38]. The powerful effect of VS by MD of NCs databases on different targets, including DNA, was reviewed by Ma et al. [39]. Ambure et al. [40] performed a pharmacophore-based VS followed by MD analyses on InterBioScreen's Natural Compound database in order to discover novel AChEIs [40]. The initial dataset of 47,868 NCs (available in 2012) was screened by multiple filters and a final set of 12 molecules was selected as potential AChEIs on the basis of their interaction patterns and docking scores.

To the best of our knowledge, there is no comprehensive study on all available databases of NCs for potential AChE inhibitory activity via molecular docking. Here, we report an MD-based VS of 11 ZINC12 databases of NCs (~150,000 compounds) for AChE affinity. The compounds were subsequently screened for blood brain barrier (BBB) permeability, gastrointestinal (GI) absorption, drug-likeness, lead-likeness, and PAINS (Pan Assay INterference Structures) by SwissADME online server tool [41]. Next, the eligible compounds were visually inspected according to their size and position within the binding pocket. MDSs were performed on the hit compounds in order to evaluate the stability of the complexes. The final set of 10 selected hits was tested experimentally.

2. Results

2.1. Virtual Screening by Molecular Docking

Almost 150,000 NCs were subject to VS based on the crystallographic structure of human-recombinant AChE (*rh*AChE, pdb id: 4EY6, R = 2.40 Å) [6]. The NCs were collected from 11 databases freely available on the ZINC12 platform: AfroDb_NP, AnalytiCon_DB, HerbalIngredients_DB, HIT_DB, IBScreen_NP, Indofine_NP, NPACT_DB, Nubbe_NP, Specs_NP, TCM_DB_Taiwan, and UEFS_NP. The docking protocol is described in Materials and Methods. The pose with the highest ChemPLP score out of 100 runs was considered for each ligand. Only compounds with docking score equal to or higher than 70 were considered as AChE binders. This cutoff value was chosen to be close to that derived for GAL (72.11) with an RMSD of 0.215 Å.

2.2. ADME Filtering and Visual Inspection

A three-step filtering was applied for hit selection (Figure 1). The first filter was blood—brain barrier (BBB) permeability, a necessary requirement for activity in the brain. It was assessed by the SwissADME server [41]. The number of ligands that passed this step was 40,613. In the next step, eight additional SwissADME filters were applied: five for drug-likeness (rules of Lipinski, Ghose, Veber, Egan and Muegge), one for gastrointestinal (GI) absorption, one for PAINS allerts, and one for lead likeness. Only 8315 of NCs fulfilled all eight criteria. At the last step, a visual inspection of the binding poses within the protein binding site was performed along with measuring the size of the aromatic moiety occupying the CAS. Only ligands bound near the PAS or deeply in the CAS with aromatic rings sized at least 5 Å in diameter between two terminal heavy atoms were selected. Thus, at the end of this three-step filtering, only 215 molecules remained. The compounds were checked for available vendors, and 32 non-GAL type molecules from 23 structural groups were selected for further analysis (Table S1). They were numbered from 1 to 34, including two GAL derivatives (**10** and **11**).
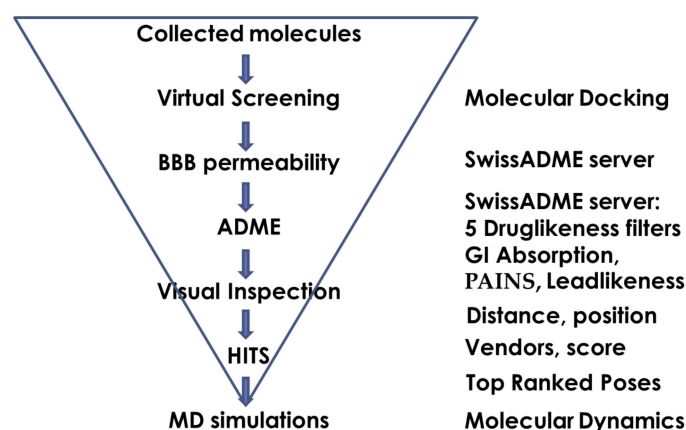
Figure 1. Hit selection by docking-based VS and ADME filtering.

2.3. Molecular Dynamics Simulatioins and Trajectory Analyses

The stability of the complexes formed between the 32 hits and the AChE was tested by 1 μs molecular dynamics simulation. Initially, the stability of the complexes was inspected visually. In 11 complexes, the ligands almost exited the BS (3, 4, 6, 24, 27, and 30) or occupied an allosteric site, and CAS remained accessible (8, 12–15). In the rest of the 21 complexes, the ligands remained in the BS during the whole simulation with ligand RMSD < 1.5 Å and protein RMSD < 2.5 Å. Five of the ligands had RMSD up to 0.5 Å (16, 31–34), for 10 of them the RMSDs varied between 0.5 and 1 Å (1, 7, 18, 19, 20, 22, 25, 26, 28, 29), and 6 molecules had RMSDs between 1 and 1.5 Å (2, 5, 9, 17, 21, 23). The protein Cα RMSDs remained below 2.5 Å, confirming the stability of the systems (Figure S1). The protein Cα RMSFs (root-mean-square fluctuations) showed that the most dynamic residues

belong to the unstructured regions on the surface between the 76th and 84th and 384th and 388th positions, around the capped chain breaks at 255th and 491th positions, and to both termini (Figure S1).

The convergence of MM-GBSA energies (ΔH) was assessed over the production phase (Figure S2). In the absence of bridging solvent molecules [42], the enthalpies converged within 100 ns and ranged between -25 and -55 kcal/mol (Figure S2). In the presence of solvent molecules, the convergence of ΔH_{solv} took longer than 100 ns and had values ranging between -30 and -66 kcal/mol (Figure S2).

Three criteria were applied in the final selection of hits for experimental testing among the 21 NCs: sum of ChemPLP score and the module of ΔH_{solv}, single vendor, and price for 1 mg (Table S2). The final set of 10 NCs selected for anti-AChE testing is given in Table 1.

Table 1. ChemPLP score, $\Delta H_{solv,avg}$, sum of their modules, and anti-AChE and antioxidant activities of the selected NCs are presented. GAL is the reference AChE inhibitor and butylhydroxytoluene (BHT) is the reference antioxidant. The IC50 and ABTS values were measured in triplicate, and the results are presented as means $\pm$ SD.

Compund	ChemPLP	$\Delta H_{solv, avrg}$, kcal/mol	ChemPLP + $|\Delta H_{solv, avrg}|$	IC_{50}, mM	ABTS (%)
5	85.0500	-30.8296	115.8796	>10	na
9	85.9159	-65.8063	151.7222	1.8 ± 0.75	6.43 ± 0.85
16	76.7413	-45.8669	122.6082	na	95.82 ± 0.21
17	82.7631	-34.3182	117.0813	>10	na
18	79.0189	-41.3130	120.3319	na	na
21	82.7599	-59.1422	141.9021	1.2 ± 0.19	34.68 ± 1.27
22	84.6421	-44.4386	129.0807	0.39 ± 0.16	na
25	77.6389	-42.3505	119.9894	Na	na
28	73.5909	-55.8388	129.4297	0.62 ± 0.14	70.55 ± 0.85
29	77.5505	-60.2032	137.7537	5.7 ± 3.50	80.94 ± 0.94
GAL	72.1100	-45.5914	117.7014	0.002 ± 0.0003	
BHT					92.38 ± 0.21

na—not active.

2.4. AChE Inhibitory Activity

The AChE activity of the selected 10 NCs was measured by Ellman's method as described in Materials and Methods. The IC_{50} values are given in Table 1. Five compounds showed $IC_{50} < 10$ mM. Their structures are given in Figure 2. Two of them, **22** and **28**, have activity in the micromolar range, another two, **9** and **21**, have activities between 1 and 2 mM, and the fifth, **29**, has an activity above 5 mM. All of them are less active than GAL with $IC_{50} = 2$ µM.
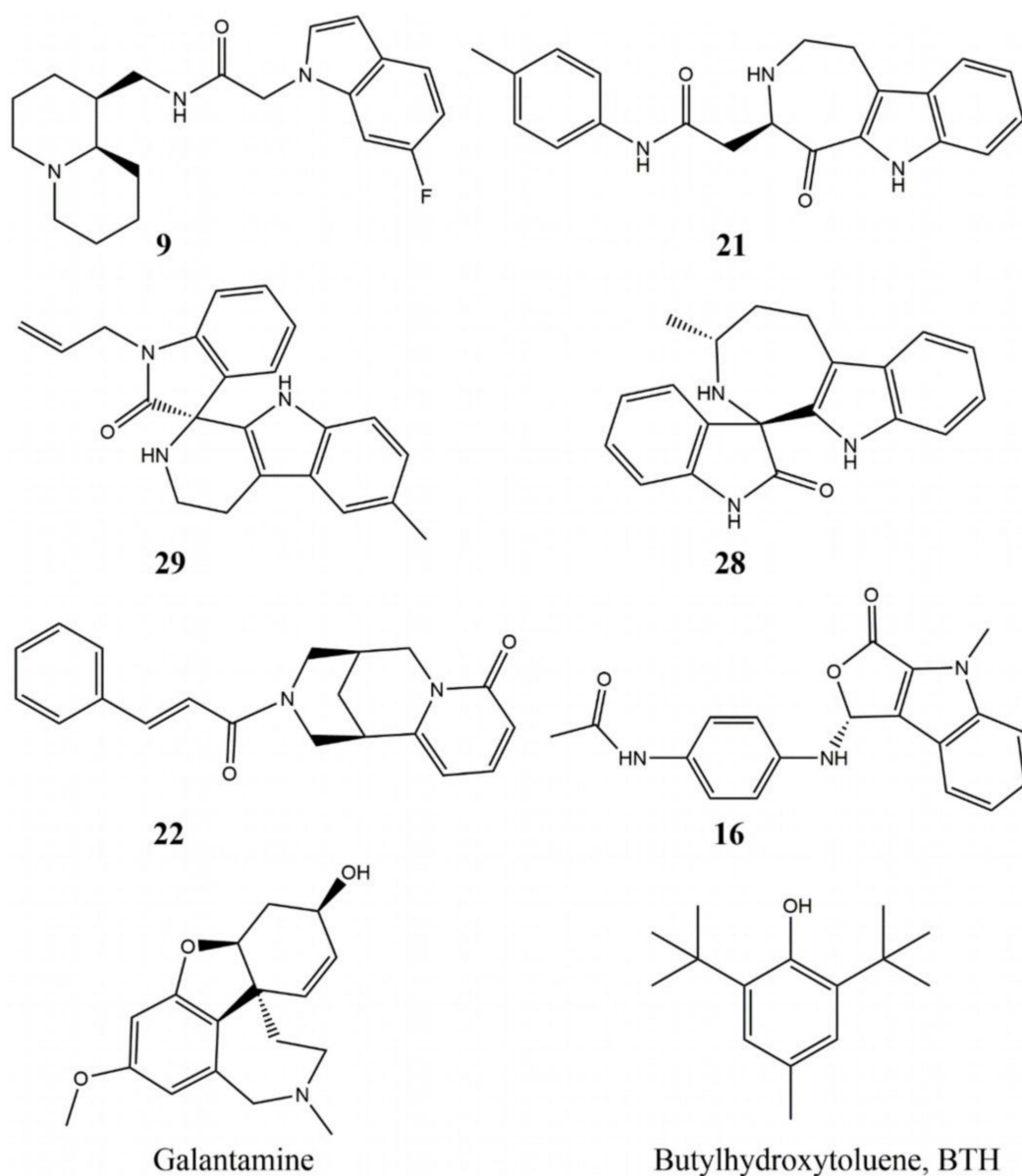
Figure 2. Structures of the novel AChE inhibitors, discovered in the present study: **9** (N-{[(1S,9aR)-octahydro-1H-quinolizin-1-yl]methyl}-2-(6-fluoro-1H-indol-1-yl)acetamide), **21** (N-(4-methylphenyl)-2-{5-oxo-1H,2H,3H,4H,5H,6H-azepino [4,5-b]indol-4-yl} acetamide), **29** (6′-methyl-1-(prop-2-en-1-yl)-1,2,2′,3′,4′,9′-hexahydrospiro[indole-3,1′-pyrido [3,4-b]indol]-2-one), **28** (3-methyl-1′,2′,3,4,5,10-hexahydro-2H-spiro[azepino [3,4-b] indole-1,3′-indol]-2′-one), **22** ((1S,9R)-11-[(2E)-3-phenylprop-2-enoyl]-7,11-diazatricyc lotrideca-2,4-dien-6-one), **16** ((R)-N-(4-((4-methyl-3-oxo-3,4-dihydro-1H-furo [3,4-b] indol-1-yl) amino)phenyl)acetamide), and the two positive controls —galantamine (GAL) and butylhydroxytoluene (BHT).

2.5. Antioxidant Activity. ABTS Radical Scavenging Activity

As the anti-AChE activity in vivo is associated with increased oxidative stress [43,44], the antioxidant potential of the selected hits was tested as well as described in Materials and Methods. It is given in Table 1 as % ABTS radical scavenging with BHT as a positive control. Two of the hits—**9** and **21**—showed weak ABTS activity of 6.43% and 34.68%, respectively. Compounds **28** and **29** showed high antioxidant activity (80.94% and 70.55%, resp.), while compound **16** showed significant activity of 95.82% comparable to and even higher than the positive control BHT (92.38%).

3. Discussion

About 150,000 NCs available in 11 databases at ZINC12 were subject to virtual screening via molecular docking against AChE. The applied docking protocol was previously optimized and used to predict new AChE inhibitors that were experimentally proven [45–51]. The compounds were screened for BBB permeability, drug-likeness filters, GI absobtion, PAINS, and lead-likeness. Visual inspection of ligand positions within the binding site of AChE followed by size measurement of the condensed ring moiety located at CAS led to a selection of 215 eligible compounds. From them, 32 non-galanthamine type molecules with the highest ChemPLP docking score and available vendor were selected. The stability of their complexes with AChE was estimated via 1 μs molecular dynamics simulation. Twenty one molecules formed stable complexes, and the ΔH values with and without solvent molecules were calculated. Ten molecules from the same vendor with prices up to USD 100 per 1 mg were selected for experimental testing. Five of them showed anti-AChE activity in the micro- to low millimolar range. They are **9**, **21**, **22**, **28**, and **29**.

In MM-PBSA and MM-GBSA calculations, the magnitude of the resultant ΔH values is sensitive to the choice of atomic radii and nonpolar decomposition scheme [52], whereas the relative energies (relative to each other) are not [42,52]. Thus, while the absolute ΔH values would be different using, for example, bondi and mbondi2 radii, the relative ranking of the compounds by ΔH would be nearly unaffected because all compounds would experience an almost identical amount of error during the calculations. Because the parameters for enthalpy calculations are the same for all complexes, all ΔH values are overestimated by a similar amount, which cancels out in the relative rankings. For example, if compound A scores significantly better than B using bondi radii, it will score better using any other set of atomic radii or decomposition scheme, as long as the same calculation scheme is applied to both compounds. It is precisely this property of relative free energy calculations that enables virtual high-throughput screening. As we aim to screen a large library of compounds, we require a rapidly computable, cheap descriptor of the affinity of the different ligands for the target protein rather than a detailed analysis of the different protein—ligand complexes [53–56]. The efficacy of our protocol is demonstrated by the high success rate (5 actives out of 10 experimentally tested molecules or 50%), which is orders of magnitude higher than the hit rate of randomly selecting compounds (usually around 0.1–1%) [57]. In Figure 3 and Table 2, we present the energetic components for the studied protein–ligand complexes and briefly discuss them below.
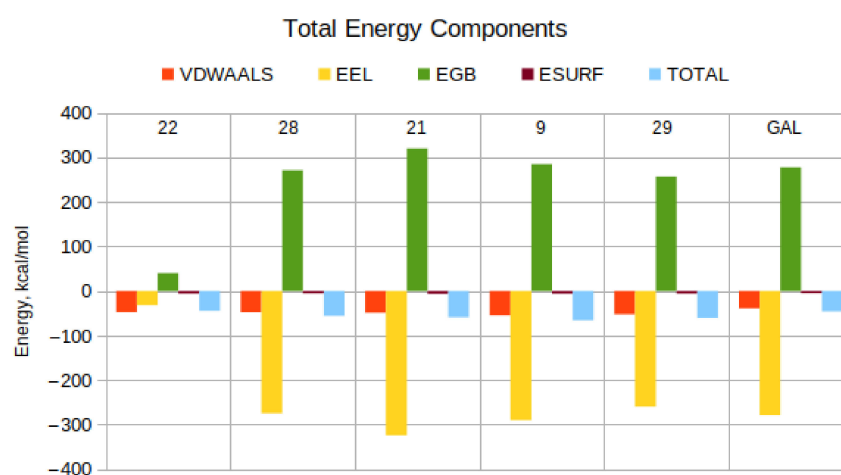

Figure 3. Total energy components of each ligand complexed with AChE. The positive control is GAL. The van der Waals and electrostatic interaction energies are denoted as VDWAALS and EEL, respectively. The polar and non-polar solvation energies are denoted as EGB and ESURF, correspondingly. The total energy of binding is denoted as TOTAL.

Table 2. Energy components (E_{VDW}—van der Waals and E_{EL}—electrostatic interaction energies; E_{GB}—polar and E_{SURF}—non-polar solvation energies solvation energies; TOTAL—total energy of binding) of the ligands complexed with the enzyme. The reference AChE inhibitor is GAL.

Compound	E_{VDW} Kcal/Mol	E_{EL} Kcal/Mol	E_{GB} Kcal/Mol	E_{SURF} Kcal/Mol	TOTAL Kcal/Mol	$E_{EL\,+\,EGB,}$ Kcal/Mol
22	−47.15	−31.53	40.20	−5.96	−44.44	8.67
28	−47.40	−274.18	271.14	−5.39	−55.84	−3.05
21	−48.46	−324.22	320.09	−6.55	−59.14	−4.13
9	−54.68	−289.90	284.96	−6.18	−65.81	−4.95
29	−52.21	−259.20	257.11	−5.91	−60.20	−2.08
GAL	−39.18	−278.77	277.42	−5.06	−45.59	−1.35

The most active compound **22** is the only one that is not charged at physiological pH. Therefore, its van der Waals (E_{VDW}), electrostatic (E_{EL}), and polar (E_{GB}) solvation values are in a similar range. All other tested compounds, including GAL, have a charge +1 at physiological pH. As expected, their electrostatic and polar solvation contributions are dominant. It is evident, however, that for each compound, these values are very close and almost cancel each other out. Thus, the main contribution to the total binding energy is due to the E_{VDW} term. The non-polar solvation contribution (E_{SURF}) is essentially always small and similar for all compounds.

Additional per-residue energy decomposition analysis for the studied compounds was performed, as depicted in Figure 4. It can be seen that in the case of compound **22**, Gly121 from the oxyanion sub-site, followed by Tyr337 from the anionic domain, considerably contributed to the binding energy. Moreover, Trp86 and Phe338 from the anionic sub-site, Gly120 and Gly122 from the oxyanion pocket, and His447 from the CAS contribute to the binding energy. His447 had a significant contribution to the total energy of ligand **28** to AChE, followed by Trp86, Gly120, Gly121, and Tyr337. In the case of compound **21**, a considerable contribution to the binding energy comes from Asp74 from the PAS, followed by Trp86, Tyr341 (PAS), and His447; a sizeable contribution to the binding energy of **9** stems from Trp86, followed by Gly121, Glu202, and Tyr337. The main contributing residue to the total binding energy for compound **29** and the enzyme is Trp86 followed by Gly121 and Glu202. The per-residue energy decomposition for the positive control, GAL, reveals that Trp86, Gly121, Glu202, and Tyr337 are the most highly contributing ones.


(A)

(B)

(C)

(D)

Figure 4. *Cont.*

(E)

(F)
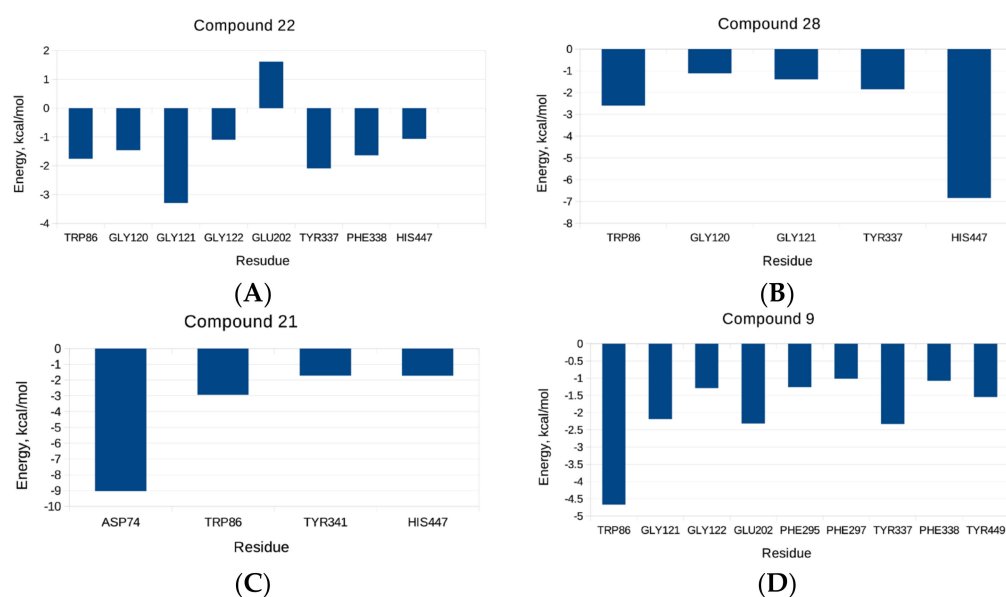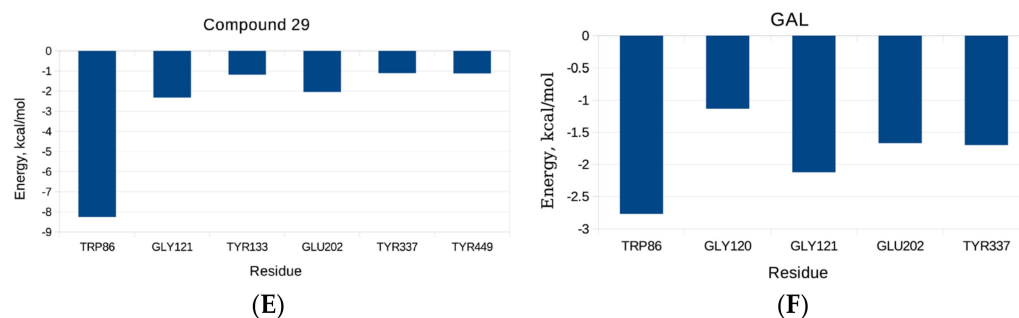
Figure 4. Energy decomposition per residue of predicted compounds (**A**) **22**, (**B**) **28**, (**C**) **21**, (**D**) **9**, (**E**) **29,** and (**F**) GAL. The energy contribution larger than 1 kcal/mol is displayed.

To gain further insight into the intermolecular interactions between the ligands and the enzyme during the course of the production, dynamics were analyzed using cpptraj V4.14.0 [58]. Compound **22** forms in three hydrogen bonds. Two of them are formed between the O atom from the carbonyl group of the linker and H atoms at N-terminus of Gly121 and Gly122 (Figures 5A and S3A,B). The third hydrogen bond occurs between the O atom from the carbonyl group from the pyridin-2-one moiety of **22** and H atom from the hydroxyl group of Tyr337 (Figures 5A and S3C). The distance between the pyridin-2-one ring of **22** and indole part of Trp86 is appropriate for a π–π contact (Figures 5A and S3D). Distances between atoms during the course of simulation are shown in Figure S3A–D.
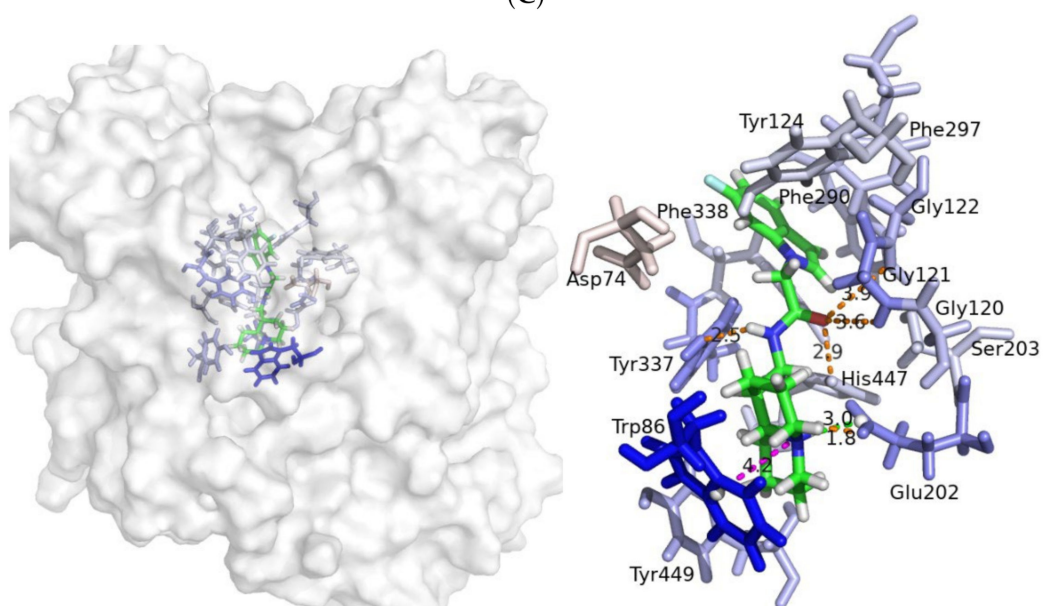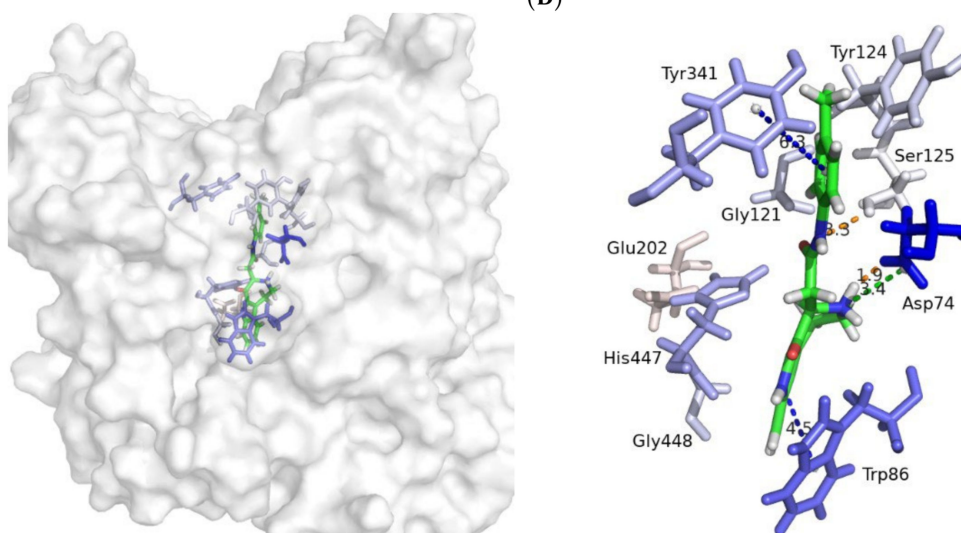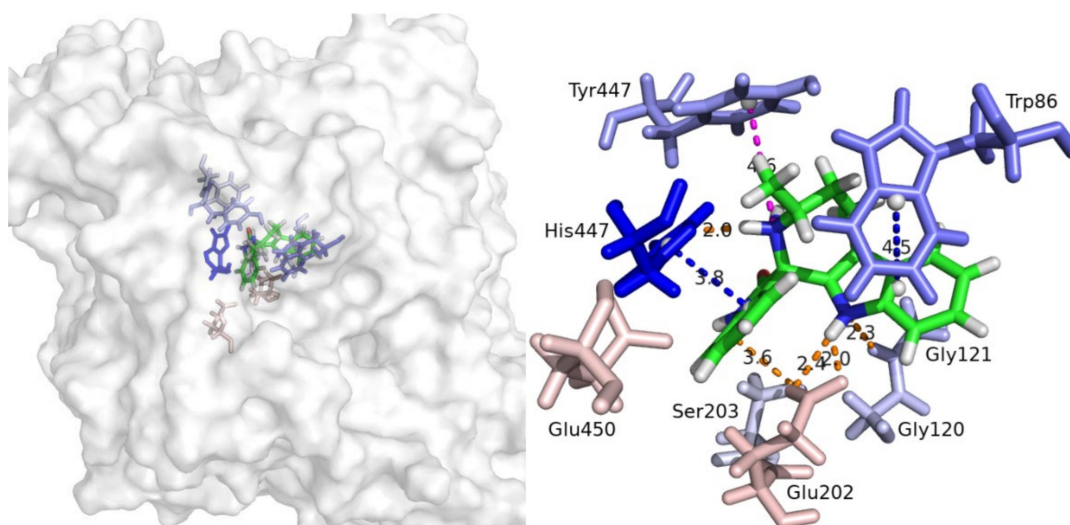

(A)

Figure 5. *Cont.*

(**B**)

(**C**)

(**D**)

Figure 5. *Cont.*

(**E**)

(**F**)
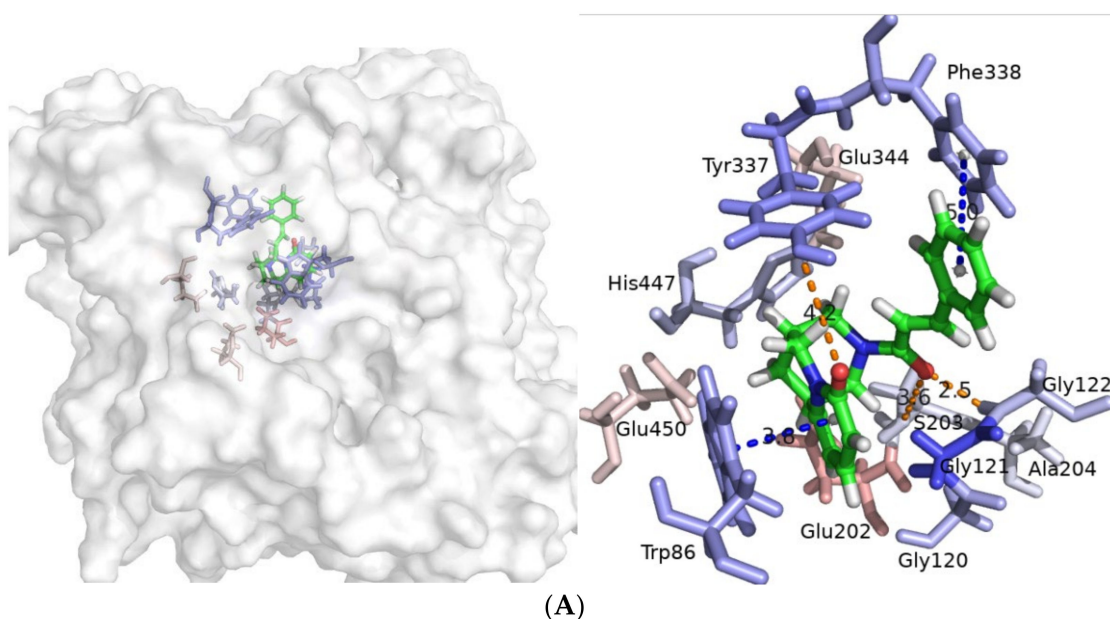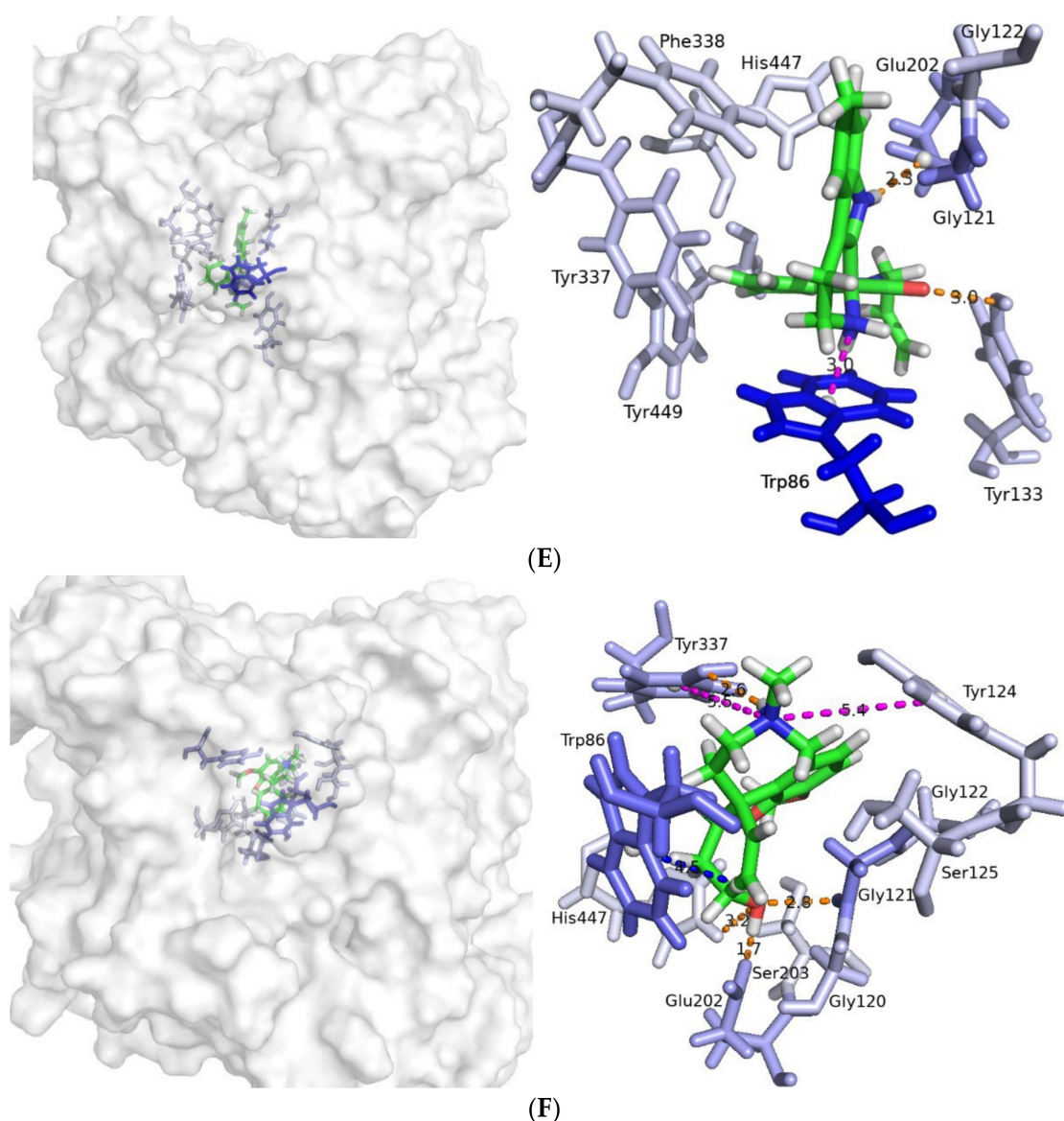
Figure 5. Intermolecular interactions between AChE and compound (**A**) **22** (in 329.8 ns), (**B**) **28** (in 486.4 ns), (**C**) **21** (in 988.4 ns), (**D**) **9** (in 557.6 ns), (**E**) **29** (in 654.8 ns), and (**F**) GAL (364.8 ns). Hydrogen bonds are denoted as orange dashes. Distances between center of mass of π–π or π–p electrons, prerequisite for π–π stacking or π–p contact, are denoted in blue dashes. Cation–π distances are presented in magenta. Salt bridges are denoted with green dashes. Distances are presented in Å. Residues are colored according to their energy contribution—blue colored ones favor the binding, while red colored do not favor it. More saturated color indicates higher contribution. Ligands are colored by element.

The complex with compound **28** is stabilized via six hydrogen bonds during molecular dynamics. The NH group at the indole moiety acts as a hydrogen bond acceptor and donor with the N-terminus from Gly121 and the carboxyl group from Glu202, respectively (Figures 5B and S4A,B). Similarly, the OH group from Ser203 takes part in two short-lasting hydrogen bonds with NH and CO groups from the indolinone part of **28** (Figures 5B and S4C,D). The N atom at His447 forms hydrogen bonds with both H atoms at the quaternary ammonium group from the ligand (Figures 5B and S4E,F). The distance between the positively charged ammonium atom and center of mas of Tyr337 is a precondition for a cation–π interaction (Figures 5B and S4G). Centers of mass of indole moieties of Trp86 and **28** are at an appropriate distance for π–π contact (Figures 5B and S4H). The

distance and position between the centers of mass of His447 and the indolinone part of **28** are a prerequisite for stable π–π stacking observed for a long period during the simulation (Figures 5B and S4I). Distances between atoms during the production dynamics are shown in Figure S4A–I.

A salt bridge is formed during the simulation between the carboxyl group from Asp74 and the quaternary ammonium group from ligand **21** (Figures 5C and S5A,B). One hydrogen bond is formed between the H atom of the side chain hydroxyl group of Ser125 and an O atom from a CO group from the linker (Figures 5C and S5C). Indole moiety from Trp86 is appropriately located for the formation a π–π contact with the indole part from ligand **21** (Figures 5C and S5D). Terminal benzene ring of **21** reaches Tyr341 from PAS, where a π–π interaction can be formed (Figures 5C and S5E). Distance plots in the course of the simulation are presented in Figure S5A–E.

In the case of compound **9**, four hydrogen bonds and one salt bridge stabilize the complex with the enzyme (Figure 5D). A salt bridge is formed between the carboxyl group from Glu202 and the quaternary ammonium group (Figures 5D and S6A,B). Three hydrogen bonds occurred during the simulation between the O atom at the CO group from the ligand's linker and H atoms at N-terminus of Gly121 and Gly122, and one with H atom from His447 (Figures 5D and S6C,D,F). The oxygen atom of the Tyyr337 hydroxyl takes part in the fourth hydrogen bond with an H atom from the linker amino group (Figures 5D and S6E). The distance between the indole part from Trp86 and the positively charged ammonium atom is appropriate for a cation–π contact (Figures 5D and S6G). Figure S6A–G shows the respective distance plots.

Two hydrogen bonds are formed between compound **29** and the enzyme. The first one is between the hydroxyl hydrogen from Tyr133 and a O atom from indolinone moiety's carbonyl group. The second one is between carboxyl group from Glu202 and the amino hydrogen from the indole part of the molecule (Figures 5E and S7A,B). The distance between the center of mass of the indole moiety from Trp86 is appropriate for a cation–π interaction with the positively charged ammonium atom of ligand **29** (Figures 5E and S7C). Distance plots are presented in Figure S7A–C.

Additionally for comparison, we analyzed the interactions between the positive control GAL and AChE (Figure 5F). Four hydrogen bonds stabilize the complex between both partners. In three of them, O atom from GAL's OH group takes part with Gly121, Glu202, and His447, respectively (Figures 5F and S8A–C). The fourth one is formed between the O atom at OH from Tyr337 and the hydrogen atom in the quaternary ammonium group (Figures 5F and S8D). The centers of mass of the benzene ring from Tyr124 and Tyr337 are at appropriate distances for cation–π contacts (Figures 5F and S8E,F). The distance between the center of mass of the indole moiety from Trp86 and the double bond from GAL is a prerequisite for π–π interaction (Figures 5F and S8G). For all of the discussed ligands, multiple steric interactions stabilize the complexes during simulation.

Compounds **9** and **22** are quinolizidine-type alkaloids. Compound **9** is a lupinine derivative containing terminal indole moiety, while compound **22** is a N-substituted cytisine derivative with terminal phenyl ring. It has been shown that lupinine and its tetramethylammonium derivative are reversible inhibitors of AChE [59]. Cytisine is used in smoking cessation [60], but it does not inhibit AChE and BChE [61]. Additionally, quinolizidine alkaloids are known to bind to nicotinic and muscarinic acetylcholine receptors (nAChR and mAChR), as lupinine binds preferably to mAChR, while cytisine binds preferably to nAChR [62]. Hupersine A, isolated from *Huperzia serrata*, is a quinolizidine-type alkaloid acting as a reversible AChE inhibitor and NMDA receptor antagonist [63–66].

Compound **29** is a dicorynamine derivative. Dicorynamine is a β-carboline alkaloid isolated from *Dicorynia guianensis* Amsh heartwood [67]. It has been found that the crude extract of alkaloids demonstrates the maximum scavenging activity in the ABTS model with IC_{50} = 90.07 μg/mL compared to the positive control ascorbic acid (IC_{50} = 105.90 μg/mL) [67]. In our ABTS study, the dicorynamine derivative, **29**, showed 80.94% ABTS activity, which is close to the positive control BHT, 92.38% (Table 1).

Compounds **21** and **28** are indole-containing compounds. Their structures partially resemble the structure of the indole alkaloid ibogaine found in *Tabernaemontana* species of the Apocynaceae family. Ibogaine has been extensively studied for anti-addictive properties, but clinical trials failed due to cardiotoxicity [68]. Additionally, ibogain-type alkaloids like catharanthine and coronaridine congeners have been found to selectively inhibit the nAChRs and Cav2.2 channels, and to potentiate GABA A receptors [69–72]. Ibogaine and coronaridine are NMDA receptor antagonists, with $K_i = 1.1$ µM and $K_i = 6.2$ µM, respectively [73].

4. Materials and Methods

4.1. Virtual Screening by Molecular Docking

Approximately 150,000 natural compounds collected from 11 freely available databases in ZINC12 were screened virtually by molecular docking. The structures were docked into the X-ray structure of recombinant human acetylcholinesterase (rhAChE, pdb id: 4EY6, R = 2.40 Å) [6]. The docking simulations were performed with GOLD v.5.2.2 [CCDC Ltd., Cambridge, UK] using a previously described and optimized-for-this-system protocol [45–51]. The following settings were used: scoring function ChemPLP, rigid protein, flexible ligand, and a radius of the binding site of 6 Å around the crystallographic structure of GAL. For each ligand, 100 poses were generated. The structural water molecule HOH846B, forming bridging interactions between the crystallographic GAL and enzyme, was excluded from the docking calculations due to the diversity of the screened ligand structures. The highest scored pose for each ligand was considered. The protocol was validated as the crystallographic structure of GAL was removed from the complex and redocked again at the described settings.

4.2. ADME Filters

The tested compounds were screened by several ADME filters. The BOILED-Egg (Brain Or Intestinal EstimateD permeation) method based on the lipophilicity and polarity of small molecules [74] implemented in the SwissADME server [41] was used to predict the BBB permeability of the ligands. Lipinski's filter, also known as the 'rule of five', is based on experimental and computational approaches to estimate solubility and permeability in drug discovery [75]. A knowledge-based approach for qualitative and quantitative characterization of known drug databases is used in the Ghose's filter [76]. The Veber's filter is based on two criteria: number of rotatable bonds and polar surface area, which are in a good correlation with the experimental oral bioavailability data for over 1100 drug candidates [77]. A statistical model for the recognition of passive intestinal absorption is applied in the Egan's filter [78]. The Muegge's criterium presents a pharmacophore point filter using so called "chemical wisdom" that is unbiased from fitting the structural content of specific drug databases to prediction models [79]. The GI absorption prediction is based on the BOILED-Egg method [74]. PAINS alerts help in the identification of frequent hitters or promiscuous compounds in many biochemical high throughput screens based on substructural features [80]. Liead-like combinatorial libraries designed by Teague et al. are applied in the lead-likeness filter [81].

4.3. Visual Inspection

The molecules that passed the ADME filters were visually inspected by two criteria: position within the binding gorge, namely if the ligand is placed in the binding site near the PAS or deeply in the CAS; and a size of at least 5 Å for the aromatic moiety was chosen as a requirement to retain the ligand in the binding site. The size was defined as the distance between two terminal heavy atoms of the aromatic ring placed in CAS. The size of the aromatic moiety of GAL in CAS is 6.033 Å.

A mandatory condition for hit selection was the vendor availability and ChemPLP score higher than that of GAL.

4.4. Molecular Dynamic Simulations and Trajectory Analyses

4.4.1. System Preparation

The coordinates of pdb id: 4EY6 were used as initial ones for the complex between AChE and GAL [6]. The structural water molecule HOH846B was kept for all MD simulations. As the X-ray AChE structure contains missing regions between residues 258 and 262 as well between 491 and 496, the Ace and NMe caps were added at both ends as well as at both terminal residues of the protein chain. Missing chain regions are far from the ACh binding site on AChE and do not influence the final results. The protein chain was solvated in a truncated octahedral box with TIP3P water [82] as a saline, as the system was kept neutral. The initial coordinates for the selected hit compounds were taken from the docking calculations. Ligand protonation states and charges at physiological pH were used as the pK_a values were predicted using ACD/logD tool (Advanced Chemistry Development, Inc., ACD/Labs). Ligand parameters were obtained using the general Amber force field (GAFF 2.11) [83] with AM1-BCC charges [84].

4.4.2. Molecular Dynamic Simulations

The solvated systems were subject to energy minimization, then heated to 300 K for 1 ns, followed by 1 ns of constant pressure density equilibration. Next, the systems were equilibrated for 1 ns under constant temperature (300 K) and pressure (1 bar), using the Langevin thermostat [85] and Berendsen barostat [86], respectively. They were simulated for 1000 ns (1 μs) of production dynamics with the ff14SB force field [87] under periodic boundary conditions. Frames were saved every 200 ps (0.2 ns) for a total of 5000 per trajectory, to be used in subsequent analysis.

4.4.3. Trajectory Processing and MM-GBSA Calculations

The stability of the systems was evaluated via root-mean-square deviations (RMSD) for ligand-heavy atoms, protein carbon alpha ($C\alpha$), and root-mean square-fluctuations (RMSF) with respect to the starting coordinates for protein $C\alpha$ atoms with cpptraj V4.14.0 [58]. For each complex trajectory, the enthalpy of binding between the AChE and the ligand (ΔH) was computed with the MMPBSA.py tool [88], part of the Amber18 package. We used the end-state free energy method, MM-GBSA (molecular mechanics-generalized Born surface area), which includes an implicit solvent analogous to MM-PBSA (molecular mechanics Poisson–Boltzmann surface area) but is computationally cheaper than MM-PBSA [42].

4.5. AChE Inhibitory Activity

The compounds selected for testing were purchased from InterBioScreen Ltd.

The microplate assay used for measuring AChE inhibitory activity was performed in 96-well plates using a modified method of Ellman et al., 1961 [89], as described by López et al., 2002 [90]. Acetylthiocholine iodide (ATCI) in solution with 5,5′-dithiobis(2-nitrobenzoic acid) (DTNB) was used as a substrate for the acetylcholinesterase from *Electrophorus electricus* (Sigma-Aldrich, Darmstadt, Germany). All compounds were tested at concentrations from 10^{-2} to 10^{-8} M. Fifty microliters of AChE (0.25 U/mL) dissolved in phosphate buffer (8 mM K_2HPO_4, 2.3 mM NaH_2PO_4, 0.15 M NaCl, pH 7.5) and 50 μL of the samples dissolved in the same buffer were added to the wells. The plates were incubated for 30 min at room temperature before the addition of 100 μL of the substrate solution (0.04 M Na_2HPO_4, 0.2 mM DTNB, 0.24 mM ATCI, pH 7.5). The absorbances were read in a microplate reader (BIOBASE, ELISA-EL10A, China) at 405 nm after 3 min. Enzyme activity was calculated as inhibition percentage compared to an assay using a buffer instead of inhibitor. GAL was used as a positive control. The AChE inhibitory data were then analyzed with the software package Prism 9 (Graph Pad Inc., San Diego, CA, USA). The IC_{50} values were measured in triplicate and the results are presented as means $\pm$ SD.

4.6. Antioxidant Activity. ABTS Radical Scavenging Activity

2,2′-azinobis-(3-ethylbenzothiazine-6-sulfonic acid) (ABTS), potassium persulphate, and butylhydroxy toluol (BHT) were purchased from Sigma-Aldrich. For ABTS assay, the procedure followed the method of Grochowski et al. [91] with some modifications. The stock solutions included 7 mM ABTS solution and 2.4 mM potassium persulphate solution. The working solution was then prepared by mixing the two stock solutions in equal quantities and allowing them to react for 14 h at room temperature in the dark. The solution was then diluted by mixing 2 mL ABTS solution with 50 mL methanol to obtain an absorbance of 0.705 ± 0.05 units at 734 nm using a Shimatzu 1203 UV-VIS spectrophotometer (Japan). A fresh ABTS solution was prepared for each assay. One millimeter of each com-pound (125 μL) was allowed to react with 1850 μL of the ABTS solution, and the absorbance was taken at 734 nm after 7 min. The control contains 125 μL methanol and 1850 μL of the ABTS solution. All determinations were performed in triplicate (n = 3). The results were expressed as % ABTS activity, using the following equation: % ABTS radical scavenging activity = $((A_{control} - A_{sample})/A_{control}) \times 100$, where $A_{control}$ is the absorbance of the control, while A_{sample} is the absorbance of the sample. Butylhydroxytoluene (BHT) (1 mM in MeOH) was used as a positive control.

5. Conclusions

In the present study, five novel naturally originating hits were discovered by multistep virtual screening as promising AChE inhibitors. Two of them (**9** and **22**) are quinolizidine-type alkaloids, another two (**21** and **28**) belong to the indole-type alkaloid family, and one (**29**) is a β-carboline-type alkaloid. Their anti-AChE activities range from 0.39 to 5.7 mM. Additionally, **29** and **28** showed high antioxidant activity. Surprisingly, one powerful antioxidant compound was discovered as well. This is compound **16**, which has no AChE activity but possesses antioxidant activity higher than that of the positive control butylhydroxytoluene. The post-MD simulation analyses reveals the structural features responsible for AChE binding. These are the carbonyl group from the linker and the pyridin-2-one moiety of **22**; the quaternary amonium groups of **9**, **21**, **22**, and **29**; the amide group from the linker; and the quinolizidine moiety of **9**. All together these findings show that the novel molecules are promising hits for further lead optimization and development.

from Gly122 and O atom in CO group from linker; (E) between O atom in CO group from Tyr337 and H atom in amino group from the linker; (F) between the H atom at NH from His447 and O atom at the carbonyl group from the linker; (G) between indole moiety from Trp86 and cation in quaternary ammonium group. Figure S7. Distance plots over the course of simulation for compound **29**. (A) between H atom in OH group from Tyr133 and O atom in CO group; (B) between COO- from Glu202 and H atom in NH group from indole part; (C) between the indole moiety of Trp86 and positively charged ammonium atom. Figure S8. Distance plots over the course of simulation for GAL. (A) between H atom in NH group from Gly121 and O atom in OH group; (B) between COO- from Glu202 and H atom in NH group from indole part; (C) between the H atom from His447 and O atom in OH; (D) between O atom in OH from Tyr337 and H atom in NH; (E) between the benzene of Tyr124 and positively charged ammonium atom; (F) between the benzene of Tyr337 and positively charged ammonium atom; (G) between the indole moiety of Trp86 and the unsaturated double bond. Table S1: Natural compounds selected as potential AChE inhipitors by docking-based virtual screening and ADME filtering. Blue lines separate the different structural groups. The stable complexes from MD simulations are denoted in bold. The galantamine derivatives are presented in italics. Table S2. A three-step procedure of molecule selection for anti-AChE screening. ChemPLP scores from docking, averaged enthalpies with included solvent interactions, and sum of both absolute values are shown. The selected compounds are given in bold.

Author Contributions: Conceptualization, M.A. and I.D. (Irini Doytchinova); methodology, M.A. and I.D. (Irini Doytchinova); data preparation, M.A. and I.D. (Ivan Dimitrov); molecular docking, M.A.; ADME screening, M.A. and I.D. (Ivan Dimitrov); molecular dynamics, M.A. and S.I.; trajectory analyses, M.A., I.D. (Ivan Dimitrov) and S.I.; visual inspection, M.A., I.D. (Ivan Dimitrov), and I.D. (Irini Doytchinova); AChE activity, B.G. and S.B.; ATBS activity, D.Z.-D.; writing—original draft preparation, M.A.; writing—review and editing, I.D. (Irini Doytchinova), S.I., I.D. (Ivan Dimitrov), S.B., B.G. and D.Z.-D.; visualization, M.A.; project administration, M.A. and I.D. (Irini Doytchinova); funding acquisition, M.A. and I.D. (Irini Doytchinova) All authors have read and agreed to the published version of the manuscript.

Institutional Review Board Statement: Not applicable.

Informed Consent Statement: Not applicable.

Data Availability Statement: Not applicable.

Conflicts of Interest: The authors declare no conflict of interest. The funders had no role in the design of the study; in the collection, analyses, or interpretation of data; in the writing of the manuscript; or in the decision to publish the results.

Sample Availability: Samples of the compounds are available from the IBScreen.

References

1. Sperling, R.A.; Aisen, P.S.; Beckett, L.A.; Bennet, D.A.; Craft, S. Toward Defining the Preclinical Stages of Alzheimer's Disease: Recommendations from the National Institute on Aging- Alzheimer's Association Workgroups on Diagnostic Guidelines for Alzheimer's Disease. *Alzheimer's Dement.* **2011**, *7*, 280–292. [CrossRef] [PubMed]
2. Ivanov, S.M.; Atanasova, M.; Dimitrov, I.; Doytchinova, I.A. Cellular Polyamines Condense Hyperphosphorylated Tau, Triggering Alzheimer's Disease. *Sci. Rep.* **2020**, *10*, 10098. [CrossRef] [PubMed]
3. Albert, M.S.; DeKosky, S.T.; Dickson, D.; Dubois, B.; Feldman, H.H.; Fox, N.C.; Gamst, A.; Holtzman, D.M.; Jagust, W.J.; Petersen, R.C.; et al. The Diagnosis of Mild Cognitive Impairment Due to Alzheimer's Disease: Recommendations from the National Institute on Aging-Alzheimer's Association Workgroups on Diagnostic Guidelines for Alzheimer's Disease. *Focus* **2013**, *7*, 270–279. [CrossRef]
4. McKhann, G.M.; Knopman, D.S.; Chertkow, H.; Hyman, B.T.; Jack, C.R., Jr.; Kawas, C.H.; Klunk, W.E.; Koroshetz, W.J.; Manly, J.J.; Mayeux, R.; et al. The Diagnosis of Dementia Due to Alzheimer's Disease: Recommendations from the National Institute on Aging-Alzheimer's Association Workgroups on Diagnostic Guidelines for Alzheimer's Disease. *Alzheimers Dement.* **2012**, *7*, 263–269. [CrossRef] [PubMed]

5. Ferreira-Vieira, H.T.; Guimaraes, M.I.; Silva, R.F.; Ribeiro, M.F. Alzheimer's Disease: Targeting the Cholinergic System. *Curr. Neuropharmacol.* **2016**, *14*, 101–115. [CrossRef]

6. Cheung, J.; Rudolph, J.M.; Burshteyn, F.; Cassidy, S.M.; Gary, N.E.; Love, J.; Franklin, M.C.; Height, J.J. Structures of Human Acetylcholinesterase in Complex with Pharmacologically Important Ligands. *J. Med. Chem.* **2012**, *55*, 10282–10286. [CrossRef]

7. Harel, M.; Schalk, I.; Ehret-Sabatier, L.; Bouet, F.; Goeldner, M.; Hirth, C.; Axelsen, P.H.; Silman, I.; Sussman, J.L. Quaternary Ligand Binding to Aromatic Residues in the Active-Site Gorge of Acetylcholinesterase. *Proc. Natl. Acad. Sci. USA* **1993**, *90*, 9031–9035. [CrossRef]

8. Ordentlich, A.; Barak, D.; Kronman, C.; Flashner, Y.; Leitner, M.; Segall, Y.; Ariel, N.; Cohen, S.; Velan, B.; Shafferman, A. Dissection of the Human Acetylcholinesterase Active Center Determinants of Substrate Specificity. Identification of Residues Constituting the Anionic Site, the Hydrophobic Site, and the Acyl Pocket. *J. Biol. Chem.* **1993**, *268*, 17083–17095. [CrossRef]

9. Ordentlich, A.; Barak, D.; Kronman, C.; Ariel, N.; Segall, Y.; Velan, B.; Shafferman, A. Functional Characteristics of the Oxyanion Hole in Human Acetylcholinesterase. *J. Biol. Chem.* **1998**, *273*, 19509–19517. [CrossRef]

10. Radic, Z.; Pickering, N.A.; Vellom, D.C.; Camp, S.; Taylor, P. Three Distinct Domains in the Cholinesterase Molecule Confer Selectivity for Acetyl- and Butyrylcholinesterase Inhibitors. *Biochemistry* **1993**, *32*, 12074–12084. [CrossRef]

11. Sussman, J.; Harel, M.; Frolow, F.; Oefner, C.; Goldman, A.; Toker, L.; Silman, I. Atomic Structure of Acetylcholinesterase from Torpedo Californica: A Prototypic Acetylcholine-Binding Protein. *Science* **1991**, *253*, 872–879. [CrossRef] [PubMed]

12. Kitz, R.J.; Braswell, L.M.; Ginsburg, S. On the Question: Is Acetylcholinesterase an Allosteric Protein? *Mol. Pharmacol.* **1970**, *6*, 108–121. [PubMed]

13. De Ferrari, G.V.; Canales, M.A.; Shin, I.; Weiner, L.M.; Silman, I.; Inestrosa, N.C. A Structural Motif of Acetylcholinesterase That Promotes Amyloid β-Peptide Fibril Formation. *Biochemistry* **2001**, *40*, 10447–10457. [CrossRef] [PubMed]

14. Johnson, G.; Moore, S. Identification of a Structural Site on Acetylcholinesterase That Promotes Neurite Outgrowth and Binds Laminin-1 and Collagen IV. *Biochem. Biophys. Res. Commun.* **2004**, *319*, 448–455. [CrossRef]

15. Johnson, G.; Moore, S. The Peripheral Anionic Site of Acetylcholinesterase: Structure, Functions and Potential Role in Rational Drug Design. *Curr. Pharm. Des.* **2006**, *12*, 217–225. [CrossRef]

16. Fisher, S.K.; Wonnacott, S. Chapter 13—Acetylcholine. In *Basic Neurochemistry*; Academic Press: Cambridge, MA, USA, 2012; pp. 258–282. [CrossRef]

17. Lockridge, O.; Quinn, D.M. 4.14—Esterases. In *Comprehensive Toxicology*, 2nd ed.; McQueen, C.A., Ed.; Elsevier: Oxford, UK, 2010; Volume 4, pp. 243–273. ISBN 978-0-08-046884-6.

18. Melnikova, I. Therapies for Alzheimer's Disease. *Nat. Rev. Drug Discov.* **2007**, *6*, 341–342. [CrossRef]

19. Knapp, M.J.; Knopman, D.S.; Solomon, P.R.; Pendlebury, W.W.; Davis, C.S.; Gracon, S.I. A 30-Week Randomized Controlled Trial of High-Dose Tacrine in Patients with Alzheimer's Disease. *JAMA* **1994**, *271*, 985–991. [CrossRef]

20. Watkins, P.B. Hepatotoxic Effects of Tacrine Administration in Patients with Alzheimer's Disease. *JAMA* **1994**, *271*, 992. [CrossRef]

21. Blackard, W.G.; Sood, G.K.; Crowe, D.R.; Fallon, M.B. Tacrine: A Cause of Fatal Hepatotoxicity? *J. Clin. Gastroenterol.* **1998**, *26*, 57–59. [CrossRef]

22. McGleenon, B.M.; Dynan, K.B.; Passmore, A. Acetylcholinesterase Inhibitors in Alzheimer's Disease. *Br. J. Clin. Pharmacol.* **1999**, *48*, 471–480. [CrossRef]

23. Batiha, G.E.-S.; Alkazmi, L.M.; Nadwa, E.H.; Rashwan, E.K.; Beshbishy, A.M.; Shaheen, H.; Wasef, L. Physostigmine: A Plant Alkaloid Isolated from Physostigma Venenosum: A Review on Pharmacokinetics, Pharmacological and Toxicological Activities. *J. Drug Deliv. Ther.* **2020**, *10*, 187–190. [CrossRef]

24. Thompson, C.A. FDA Approves Galantamine for Alzheimer's Disease. *Am. J. Health-Syst. Pharm.* **2001**, *58*, 649. [CrossRef] [PubMed]

25. Herrmann, N.; Chau, S.A.; Kircanski, I.; Lanctôt, K.L. Current and Emerging Drug Treatment Options for Alzheimer's Disease. *Drugs* **2011**, *71*, 2031–2065. [CrossRef] [PubMed]

26. Kulshreshtha, A.; Piplani, P. Current Pharmacotherapy and Putative Disease-Modifying Therapy for Alzheimer's Disease. *Neurol. Sci.* **2016**, *37*, 1403–1435. [CrossRef] [PubMed]

27. Loveman, E.; Green, C.; Kirby, J.; Takeda, A.; Picot, J.; Payne, E.; Clegg, A. The Clinical and Cost-Effectiveness of Donepezil, Rivastigmine, Galantamine and Memantine for Alzheimer's Disease. *Health Technol. Assess.* **2006**, *10*, iii–iv. [CrossRef] [PubMed]

28. Harvey, A. Natural Products in Drug Discovery. *Drug Discov. Today* **2008**, *13*, 894–901. [CrossRef] [PubMed]

29. Mukherjee, P.K.; Kumar, V.; Mal, M.; Houghton, P.J. Acetylcholinesterase Inhibitors from Plants. *Phytomedicine* **2007**, *14*, 289–300. [CrossRef]

30. Williams, P.; Sorribas, A.; Howes, M.-J.R. Natural Products as a Source of Alzheimer's Drug Leads. *Nat. Prod. Rep.* **2011**, *28*, 48–77. [CrossRef]

31. Houghton, P.J.; Ren, Y.; Howes, M.J. Acetylcholinesterase Inhibitors from Plants and Fungi. *Nat. Prod. Rep.* **2006**, *23*, 181–199. [CrossRef]

32. Murray, A.; Faraoni, M.; Castro, M.; Alza, N.; Cavallaro, V. Natural AChE Inhibitors from Plants and Their Contribution to Alzheimer's Disease Therapy. *Curr. Neuropharmacol.* **2013**, *11*, 388–413. [CrossRef]

33. Orhan, G.; Orhan, I.; Öztekin-Subutay, N.; Ak, F.; Şener, B. Contemporary Anticholinesterase Pharmaceuticals of Natural Origin and Their Synthetic Analogues for the Treatment of Alzheimer's Disease. *Recent Pat. CNS Drug Discov.* **2009**, *4*, 43–51. [CrossRef] [PubMed]

34. Choi, D.Y.; Choi, H. Natural Products from Marine Organisms with Neuroprotective Activity in the Experimental Models of Alzheimer's Disease, Parkinson's Disease and Ischemic Brain Stroke: Their Molecular Targets and Action Mechanisms. *Arch. Pharmacal Res.* **2015**, *38*, 139–170. [CrossRef] [PubMed]

35. Scotti, L.; Scotti, M.T. In Silico Studies Applied to Natural Products with Potential Activity against Alzheimer's Disease. In *Computational Modeling of Drugs against Alzheimer's Disease*; Roy, K., Ed.; Humana Press: New York, NY, USA, 2018; Volume 132, pp. 513–531.

36. Huang, L.; Su, T.; Li, X. Natural Products as Sources of New Lead Compounds for the Treatment of Alzheimer's Disease. *Curr. Top. Med. Chem.* **2013**, *13*, 1864–1878. [CrossRef] [PubMed]

37. Naaz, H.; Singh, S.; Pandey, V.P.; Singh, P.; Dwivedi, U.N. Anti-Cholinergic Alkaloids as Potential Therapeutic Agents for Alzheimer's Disease: An in Silico Approach. *Indian J. Biochem. Biophys.* **2013**, *50*, 120–125.

38. Awasthi, M.; Upadhyay, A.K.; Singh, S.; Pandey, V.P.; Dwivedi, U.N. Terpenoids as Promising Therapeutic Molecules against Alzheimer's Disease: Amyloid Beta- and Acetylcholinesterase-Directed Pharmacokinetic and Molecular Docking Analyses. *Mol. Simul.* **2018**, *44*, 1–11. [CrossRef]

39. Ma, D.-L.; Chan, D.S.-H.; Leung, C.-H. Molecular Docking for Virtual Screening of Natural Product Databases. *Chem. Sci.* **2011**, *2*, 1656–1665. [CrossRef]

40. Ambure, P.; Kar, S.; Roy, K. Pharmacophore Mapping-Based Virtual Screening Followed by Molecular Docking Studies in Search of Potential Acetylcholinesterase Inhibitors as Anti-Alzheimer's Agents. *BioSystems* **2014**, *116*, 10–20. [CrossRef]

41. Daina, A.; Michielin, O.; Zoete, V. SwissADME: A Free Web Tool to Evaluate Pharmacokinetics, Drug-Likeness and Medicinal Chemistry Friendliness of Small Molecules. *Sci. Rep.* **2017**, *7*, 42717. [CrossRef]

42. Ivanov, S.M.; Dimitrov, I.; Doytchinova, I.A. Bridging Solvent Molecules Mediate RNase A—Ligand Binding. *PLoS ONE* **2019**, *14*, e0224271. [CrossRef]

43. Milatovic, D.; Gupta, R.C.; Aschner, M. Anticholinesterase Toxicity and Oxidative Stress. *Sci. World J.* **2006**, *6*, 295–310. [CrossRef]

44. Hernández-Moreno, D.; Soler, F.; Míguez, M.P.; Pérez-López, M. Brain Acetylcholinesterase, Malondialdehyde and Reduced Glutathione as Biomarkers of Continuous Exposure of Tench, Tinca Tinca, to Carbofuran or Deltamethrin. *Sci. Total Environ.* **2010**, *408*, 4976–4983. [CrossRef] [PubMed]

45. Atanasova, M.; Yordanov, N.; Dimitrov, I.; Berkov, S.; Doytchinova, I. Molecular Docking Study on Galantamine Derivatives as Cholinesterase Inhibitors. *Mol. Inform.* **2015**, *34*, 394–403. [CrossRef] [PubMed]

46. Atanasova, M.; Stavrakov, G.; Philipova, I.; Zheleva, D.; Yordanov, N.; Doytchinova, I. Galantamine Derivatives with Indole Moiety: Docking, Design, Synthesis and Acetylcholinesterase Inhibitory Activity. *Bioorg. Med. Chem.* **2015**, *23*, 5382–5389. [CrossRef] [PubMed]

47. Stavrakov, G.; Philipova, I.; Zheleva, D.; Atanasova, M.; Konstantinov, S.; Doytchinova, I. Docking-Based Design of Galantamine Derivatives with Dual-Site Binding to Acetylcholinesterase. *Mol. Inform.* **2016**, *35*, 278–285. [CrossRef] [PubMed]

48. Doytchinova, I.; Atanasova, M.; Stavrakov, G.; Philipova, I.; Zheleva-Dimitrova, D. Galantamine Derivatives as Acetyl-cholinesterase Inhibitors: Docking, Design, Synthesis, and Inhibitory Activity. In *Computational Modeling of Drugs against Alzheimer's Disease. Neuromethods*; Roy, K., Ed.; Humana Press: New York, NY, USA, 2018; Volume 132, pp. 163–176.

49. Doytchinova, I.; Atanasova, M.; Valkova, I.; Stavrakov, G.; Philipova, I.; Zhivkova, Z.; Zheleva-Dimitrova, D.; Konstantinov, S.; Dimitrov, I. Novel Hits for Acetylcholinesterase Inhibition Derived by Docking-Based Screening on ZINC Database. *J. Enzym. Inhib. Med. Chem.* **2018**, *33*, 768–776. [CrossRef] [PubMed]

50. Stavrakov, G.; Philipova, I.; Lukarski, A.; Atanasova, M.; Zheleva, D.; Zhivkova, Z.D.; Ivanov, S.; Atanasova, T.; Konstantinov, S.; Doytchinova, I. Galantamine-Curcumin Hybrids as Dual-Site Binding Acetylcholinesterase Inhibitors. *Molecules* **2020**, *25*, 3341. [CrossRef]

51. Stavrakov, G.; Philipova, I.; Lukarski, A.; Atanasova, M.; Georgiev, B.; Atanasova, T.; Konstantinov, S.; Doytchinova, I. Discovery of a Novel Acetylcholinesterase Inhibitor by Fragment-Based Design and Virtual Screening. *Molecules* **2021**, *26*, 2058. [CrossRef]

52. Ivanov, S.M.; Huber, R.G.; Warwicker, J.; Bond, P.J. Energetics and Dynamics Across the Bcl-2-Regulated Apoptotic Pathway Reveal Distinct Evolutionary Determinants of Specificity and Affinity. *Structure* **2016**, *24*, 2024–2033. [CrossRef]

53. Shamim, A.; Abbasi, S.W.; Azam, S.S. Structural and Dynamical Aspects of Streptococcus Gordonii FabH through Molecular Docking and MD Simulations. *J. Mol. Graph. Model.* **2015**, *60*, 180–196. [CrossRef]

54. Abbasi, S.; Raza, S.; Azam, S.S.; Liedl, K.R.; Fuchs, J.E. Interaction Mechanisms of a Melatonergic Inhibitor in the Melatonin Synthesis Pathway. *J. Mol. Liq.* **2016**, *221*, 507–517. [CrossRef]

55. Azam, S.S.; Abro, A.; Raza, S. Binding Pattern Analysis and Structural Insight into the Inhibition Mechanism of Sterol 24-C Methyltransferase by Docking and Molecular Dynamics Approach. *J. Biomol. Struct. Dyn.* **2015**, *33*, 2563–2577. [CrossRef] [PubMed]

56. Raza, S.; Azam, S.S. AFD: An Application for Bi-Molecular Interaction Using Axial Frequency Distribution. *J. Mol. Modeling* **2018**, *24*, 84. [CrossRef] [PubMed]

57. Tran-Nguyen, V.-K.; Jacquemard, C.; Rognan, D. LIT-PCBA: An Unbiased Data Set for Machine Learning and Virtual Screening. *J. Chem. Inf. Modeling* **2020**, *60*, 4263–4273. [CrossRef] [PubMed]

58. Roe, D.R.; Cheatham, T.E. PTRAJ and CPPTRAJ: Software for Processing and Analysis of Molecular Dynamics Trajectory Data. *J. Chem. Theory Comput.* **2013**, *9*, 3084–3095. [CrossRef]

59. Rozengart, E.; Basova, N.E. Ammonium Compounds with Localized and Delocalized Charge as Reversible Inhibitors of Cholinesterases of Different Origin. *J. Evol. Biochem. Physiol.* **2001**, *37*, 604–610. [CrossRef]

60. Walker, N.; Howe, C.; Glover, M.; McRobbie, H.; Barnes, J.; Nosa, V.; Parag, V.; Bassett, B.; Bullen, C. Cytisine versus Nicotine for Smoking Cessation. *N. Engl. J. Med.* **2014**, *371*, 2353–2362. [CrossRef] [PubMed]

61. Orhan, I.; Naz, Q.; Kartal, M.; Tosun, F.; Sener, B.; Choudhary, M.I. In Vitro Anticholinesterase Activity of Various Alkaloids. *Z. Nat. C* **2007**, *62*, 684–688. [CrossRef] [PubMed]

62. Schmeller, T.; Sauerwein, M.; Sporer, F.; Wink, M.; Müller, W.E. Binding of Quinolizidine Alkaloids to Nicotinic and Muscarinic Acetylcholine Receptors. *J. Nat. Prod.* **1994**, *57*, 1316–1319. [CrossRef]

63. Tang, X.C.; He, X.C.; Bai, D.L. Huperzine A: A Novel Acetylcholinesterase Inhibitor. *Drugs Future* **1999**, *24*, 647. [CrossRef]

64. Wang, R.; Yan, H.; Tang, X. Progress in Studies of Huperzine A, a Natural Cholinesterase Inhibitor from Chinese Herbal Medicine[1]. *Acta Pharmacol. Sin.* **2006**, *27*, 1–26. [CrossRef]

65. Wang, B.; Wang, H.; Wei, Z.; Song, Y.; Zhang, L.; Chen, H. Efficacy and Safety of Natural Acetylcholinesterase Inhibitor Huperzine A in the Treatment of Alzheimer's Disease: An Updated Meta-Analysis. *J. Neural Transm.* **2009**, *116*, 457–465. [CrossRef] [PubMed]

66. Coleman, B.R.; Ratcliffe, R.H.; Oguntayo, S.A.; Shi, X.; Doctor, B.P.; Gordon, R.K.; Nambiar, M.P. [+]-Huperzine A Treatment Protects against N-Methyl-d-Aspartate-Induced Seizure/Status Epilepticus in Rats. *Chem. Biol. Interact.* **2008**, *175*, 387–395. [CrossRef] [PubMed]

67. Anouhe, J.-B.S.; Adima, A.A.; Niamké, F.B.; Stien, D.; Amian, B.K.; Blandinières, P.-A.; Virieux, D.; Pirat, J.-L.; Kati-Coulibaly, S.; Amusant, N. Dicorynamine and Harmalan-N-Oxide, Two New β-Carboline Alkaloids from Dicorynia Guianensis Amsh Heartwood. *Phytochem. Lett.* **2015**, *12*, 158–163. [CrossRef]

68. Koenig, X.; Hilber, K. The Anti-Addiction Drug Ibogaine and the Heart: A Delicate Relation. *Molecules* **2015**, *20*, 2208–2228. [CrossRef] [PubMed]

69. Arias, H.R.; Targowska-Duda, K.M.; Feuerbach, D.; Jozwiak, K. Coronaridine Congeners Inhibit Human A3β4 Nicotinic Acetylcholine Receptors by Interacting with Luminal and Non-Luminal Sites. *Int. J. Biochem. Cell Biol.* **2015**, *65*, 81–90. [CrossRef]

70. Arias, H.R.; Lykhmus, O.; Uspenska, K.; Skok, M. Coronaridine Congeners Modulate Mitochondrial A3β4* Nicotinic Acetyl-choline Receptors with Different Potency and through Distinct Intra-Mitochondrial Pathways. *Neurochem. Int.* **2018**, *114*, 26–32. [CrossRef]

71. Arias, H.R.; Tae, H.-S.; Micheli, L.; Yousuf, A.; Ghelardini, C.; Adams, D.J.; di Cesare Mannelli, L. Coronaridine Congeners Decrease Neuropathic Pain in Mice and Inhibit A9α10 Nicotinic Acetylcholine Receptors and CaV2.2 Channels. *Neuropharmacology* **2020**, *175*, 108194. [CrossRef]

72. Arias, H.R.; do Rego, J.L.; do Rego, J.C.; Chen, Z.; Anouar, Y.; Scholze, P.; Gonzales, E.B.; Huang, R.; Chagraoui, A. Coronaridine Congeners Potentiate GABAA Receptors and Induce Sedative Activity in Mice in a Benzodiazepine-Insensitive Manner. *Prog. Neuro-Psychopharmacol. Biol. Psychiatry* **2020**, *101*, 109930. [CrossRef]

73. Wiart, C. *Lead Compounds from Medicinal Plants for the Treatment of Cancer*; Elsevier: London, UK, 2013; ISBN 9780123983718.

74. Daina, A.; Zoete, V. A BOILED-Egg to Predict Gastrointestinal Absorption and Brain Penetration of Small Molecules. *ChemMed-Chem* **2016**, *11*, 1117–1121. [CrossRef]

75. Lipinski, C.A.; Lombardo, F.; Dominy, B.W.; Feeney, P.J. Experimental and Computational Approaches to Estimate Solubility and Permeability in Drug Discovery and Development Settings 1PII of Original Article: S0169-409X(96)00423-1. The Article Was Originally Published in Advanced Drug Delivery Reviews 23 (1997). *Adv. Drug Deliv. Rev.* **2001**, *46*, 3–26. [CrossRef]

76. Ghose, A.K.; Viswanadhan, V.N.; Wendoloski, J.J. A Knowledge-Based Approach in Designing Combinatorial or Medicinal Chemistry Libraries for Drug Discovery. 1. A Qualitative and Quantitative Characterization of Known Drug Databases. *J. Comb. Chem.* **1999**, *1*, 55–68. [CrossRef] [PubMed]

77. Veber, D.F.; Johnson, S.R.; Cheng, H.-Y.; Smith, B.R.; Ward, K.W.; Kopple, K.D. Molecular Properties That Influence the Oral Bioavailability of Drug Candidates. *J. Med. Chem.* **2002**, *45*, 2615–2623. [CrossRef] [PubMed]

78. Egan, W.J.; Merz, K.M.; Baldwin, J.J. Prediction of Drug Absorption Using Multivariate Statistics. *J. Med. Chem.* **2000**, *43*, 3867–3877. [CrossRef] [PubMed]

79. Muegge, I.; Heald, S.L.; Brittelli, D. Simple Selection Criteria for Drug-like Chemical Matter. *J. Med. Chem.* **2001**, *44*, 1841–1846. [CrossRef] [PubMed]

80. Baell, B.J.; Holloway, A.G. New Substructure Filters for Removal of Pan Assay Interference Compounds (PAINS) from Screening Libraries and for Their Exclusion in Bioassays. *J. Med. Chem.* **2010**, *53*, 2719–2740. [CrossRef]

81. Teague, S.J.; Davis, A.M.; Leeson, P.D.; Oprea, T. The Design of Leadlike Combinatorial Libraries. *Angew. Chem. Int. Ed.* **1999**, *38*, 3743–3748. [CrossRef]

82. Jorgensen, W.L.; Chandrasekhar, J.; Madura, J.D.; Impey, R.W.; Klein, M.L. Comparison of Simple Potential Functions for Simulating Liquid Water. *J. Chem. Phys.* **1983**, *79*, 926–935. [CrossRef]

83. Wang, J.; Wolf, R.M.; Caldwell, J.W.; Kollman, P.A.; Case, D.A. Development and Testing of a General Amber Force Field. *J. Comput. Chem.* **2004**, *25*, 1157–1174. [CrossRef]

84. Jakalian, A.; Bush, B.L.; Jack, D.B.; Bayly, C.I. Fast, Efficient Generation of High-Quality Atomic Charges. AM1-BCC Model: I. Method. *J. Comput. Chem.* **2000**, *21*, 132–146. [CrossRef]

85. Adelman, S.A.; Doll, J.D. Generalized Langevin Equation Approach for Atom/Solid-surface Scattering: Collinear Atom/Harmonic Chain Model. *J. Chem. Phys.* **1974**, *61*, 4242–4245. [CrossRef]

86. Berendsen, H.J.C.; Postma, J.P.M.; van Gunsteren, W.F.; DiNola, A.; Haak, J.R. Molecular Dynamics with Coupling to an External Bath. *J. Chem. Phys.* **1984**, *81*, 3684–3690. [CrossRef]

87. Maier, J.A.; Martinez, C.; Kasavajhala, K.; Wickstrom, L.; Hauser, K.E.; Simmerling, C. Ff14SB: Improving the Accuracy of Protein Side Chain and Backbone Parameters from Ff99SB. *J. Chem. Theory Comput.* **2015**, *11*, 3696–3713. [CrossRef] [PubMed]

88. Miller, B.R.; McGee, T.D.; Swails, J.M.; Homeyer, N.; Gohlke, H.; Roitberg, A.E. MMPBSA.Py: An Efficient Program for End-State Free Energy Calculations. *J. Chem. Theory Comput.* **2012**, *8*, 3314–3321. [CrossRef] [PubMed]

89. Ellman, G.L.; Courtney, K.D.; Andres, V.; Featherstone, R.M. A New and Rapid Colorimetric Determination of Acetylcholinesterase Activity. *Biochem. Pharmacol.* **1961**, *7*, 88–95. [CrossRef]

90. López, S.; Bastida, J.; Viladomat, F.; Codina, C. Acetylcholinesterase Inhibitory Activity of Some Amaryllidaceae Alkaloids and Narcissus Extracts. *Life Sci.* **2002**, *71*, 2521–2529. [CrossRef]

91. Grochowski, D.M.; Uysal, S.; Aktumsek, A.; Granica, S.; Zengin, G.; Ceylan, R.; Locatelli, M.; Tomczyk, M. In Vitro Enzyme Inhibitory Properties, Antioxidant Activities, and Phytochemical Profile of Potentilla Thuringiaca. *Phytochem. Lett.* **2017**, *20*, 365–372. [CrossRef]